Microporous and Mesoporous Materials 227 (2016) 9–15

Contents lists available at ScienceDirect

Microporous and Mesoporous Materials

journal homepage: www.elsevier.com/locate/micromeso

Optimization of the synthesis of SBA-3 mesoporous materials by experimental design

María V. Ponte, Lorena P. Rivoira, Jorgelina Cussa, María L. Martínez, Andrea R. Beltramone, Oscar A. Anunziata*

Centro de Investigación en Nanociencia y Nanotecnología (NANOTEC), Facultad Regional Córdoba, Universidad Tecnológica Nacional, Maestro López y Cruz Roja Argentina, 5016 Córdoba, Argentina

ARTICLE INFO

Article history:
Received 9 November 2015
Received in revised form
5 February 2016
Accepted 12 February 2016
Available online 18 February 2016

Keywords:
Synthesis
SBA-3
Design-response surface
Optimal synthesis conditions

ABSTRACT

SBA-3 mesoporous materials are characterized by hexagonal regular arrangements of channels with diameters >2 nm, high specific surface areas and high specific pore volumes. In the work reported herein, experimental design-response surface methodology (RSM) is used to model and optimize the synthesis conditions for SBA-3 mesoporous materials. In this study, we evaluate the influences of surfactant/silica source molar ratios, aging times, temperature and pH on the synthesis of SBA-3 mesoporous materials by analyzing the XRD intensities pertaining to the [100] signal. Response surfaces were obtained using the Box–Behnken design, and the combination of reaction parameters was optimized. By applying statistical methodology, higher levels of the objective function (XRD intensities pertaining to the [100] signal) were obtained using cetyltrimethylammonium bromide (CTAB)/tetraethyl orthosilicate (TEOS) molar ratios of 0.07 and 0.16, HCl/TEOS molar ratios of 8 and 11, reaction temperatures of 35 and 45 °C and aging times of 12–24 h. The mesoporous SBA-3 samples obtained were characterized using small-angle X-ray powder diffraction (XRD), BET, FTIR and ^{29}Si NMR-MAS, scanning electron microscopy (SEM) and transmission electron microscopy (TEM).

1. Introduction

Since the discovery of mesoporous silica [1,2] (a patent for a similar synthesis of such mesoporous silica was obtained in 1970 [3]), an explosion in the syntheses and characterizations of mesoporous oxides has occurred, initiated by the Mobil Oil Corporation Group [4,5]. Thus, there has been great scientific interest in determining the separation, catalysis and advanced materials properties of these synthetic materials [6–12]. In this regard, the morphologies of mesoporous materials combined with their internal structures are required considerations. Patarin et al. [13] have concluded that the structure formations of ordered mesoporous materials depend largely on parameters related to the specific chemistry and chemical interactions involved in each system as well as the physical conditions employed in the synthesis. The following factors are of general importance: types of inorganic material (metal, metal oxide or others); types of precursors (alkoxides or salts) and hydrolysis and condensation kinetics; types of surface active molecules (cat-, an-, or non-ionic); respective and relative concentrations of surfactants (micellar or liquid crystal) and inorganic species; pH, temperature and aging time used in each synthesis; additives (inorganic salts and organic molecules); order of mixing; types of solvents (aqueous or non-aqueous) and solvent compositions; and type of synthesis (evaporation-induced self-assembly).

Many research groups have focused on understanding the influence of synthesis parameters on the structural properties of mesostructured materials. However, most of the mechanisms proposed concern silica-based MCM-41-, SBA-15- and SBA-16-type solids; there are relatively few studies of SBA-3 materials.

SBA-3 (Santa Barbara Amorphous-3) materials are prepared using cetyltrimethylammonium (CTAB) cations, and mesopores are formed by a hexagonal array of parallel channels separated by silica walls (P6mm space group) [14]. It has been revealed that SBA-3 mesoporous silica structures contain micropores [15,16].

The aim of the present study was to determine the influence of synthetic parameters (i.e., temperature, aging time, surfactant and

* Corresponding author.
E-mail address: oanunziata@frc.utn.edu.ar (O.A. Anunziata).

http://dx.doi.org/10.1016/j.micromeso.2016.02.030
1387-1811/

acid concentration) on the structural and chemical properties of SBA-3 mesoporous materials using statistical experimental design.

'Statistical experimental design' is the process of planning an experiment such that the resulting data can be analyzed using statistical methods, thereby producing concrete and valid conclusions [17–23]. One of the main advantages of utilizing response curves is the visualization of associated responses for all experimental factors employed. The objective is to select the values of independent variables that optimize all associated responses simultaneously. Experimental design-response surface methodology (RSM) is used in the present work to model and optimize the response intensity of the XRD pattern for the [100] signal during the process of SBA-3 synthesis. In this study, a Box–Behnken design was used to analyze the influence of surfactant/silica source molar ratios, aging times, temperatures and pH values on SBA-3 synthesis to optimize the experimental design. Preparation of mesoporous silica was based on the procedure proposed by Anunziata et al. [24], using tetraethyl orthosilicate (TEOS) as the silica source and cetyltrimethylammonium bromide (CTAB) as the template. Finally, we report the optimal reaction conditions for synthesizing SBA-3 and characterize the resulting samples using XRD, BET, FTIR, NMR-MAS, SEM and TEM.

2. Experimental

2.1. Experimental design-response surface

To optimize the conditions employed in synthesizing SBA-3 materials, a Box–Behnken design was utilized. The variables considered (with regard to their effects on the XRD intensity signal characteristics of SBA-3 at [100], 2theta ~ 3°) were as follows: A) CTAB/TEOS ratio, B) HCl/TEOS ratio, C) reaction temperature, and D) aging time of the synthesis. In this regard, we investigated the following values:

(A) CTAB/TEOS molar ratio: 0.0685 – 0.1712 – 0.2740
(B) HCl/TEOS molar ratio: 4.535 – 9.068 – 13.601
(C) Temperature of synthesis: 10 – 40 – 70 (°C)
(D) Aging time of synthesis: 0 – 12 – 24 (h)

We conducted 27 Box–Behnken design experiments, in which runs were randomly performed, and the resulting data were analyzed at the 95.0% confidence level. For RSM, factorial design was utilized, and the results were adjusted using mathematical models. The stages, known as displacement stage and design, respectively, were repeated several times, during which the response surface obtained was screened in the direction of the region of the optimum point. The resulting design was analyzed using Statgraphics and Statistica software®.

2.2. Synthesis

SBA-3 samples were synthesized using tetraethyl orthosilicate (TEOS, Aldrich) as the silica source and cetyltrimethylammonium bromide (CTAB, Cicarelli) as the template. Aqueous solution containing HCl (Cicarelli, 37%) was used to adjust the pH of the reaction system.

Using the preparation procedure described in Ref. [24], we varied the temperature of the synthesis, the CTAB/TEOS molar ratio, the HCl/TEOS molar ratio and the aging time, according to the methods employed by experimental design.

In a typical synthesis, CTAB was dissolved in deionized water and acidified with HCl until a clear solution was obtained. TEOS was then added dropwise to the acidic CTAB solution, stirring at different temperatures (10, 40 and 70 °C) for 1 h, after which the solution rested (no stirring) for different aging times (0, 12 and 24 h). The molar composition of the reaction mixture was TEOS:*x* CTAB:*y* HCl:138.9H_2O, where *x* is between 0.069 and 0.27 and *y* is between 4.54 and 13.6. A white precipitate was recovered by filtration, washed with deionized water and dried overnight at 50 °C. Subsequently, the surfactant was removed in air using an initial temperature of 50 °C, which was increased at a rate of 1 °C/min to 550 °C, at which the system was maintained for another 5 h. A total of 27 samples were synthesized according to the experimental design described herein. The samples obtained under different synthesis conditions were denoted as follows: SBA-3 (CTAB/TEOS, HCl/TEOS, temperature, aging time), e.g., SBA-3a (0.069-9.07-40-0).

2.3. Characterization

X-ray diffraction (XRD) patterns were recorded using a Philips X'Pert PRO PANalytical diffractometer under Cu Kα radiation (λ = 0.154 nm). Diffraction patterns were recorded stepwise over a series of Bragg angles (2θ) ranging from 1.6 to 6, using a scanning rate of 0.02 per step and an accumulation time of 20 s. N_2 physisorption employed TriStar II 3020 V1.03 (Micromeritics Instrument Corporation) to determine the BET area average pore diameter as determined by BJH-adsorption, and pore volume. Sample fingerprints were examined using SBA wafers in KBr and analysis via a JASCO 5300 Fourier transform infrared spectrometer (FTIR). ^{29}Si MAS-NMR spectra were recorded at room temperature on a Bruker MSL-300 spectrometer, and chemical shifts were referenced to tetramethylsilane (TMS). PHILIPS-501B SEM equipment was used to determine crystal sizes and shapes. Transmission electron microscopy (TEM) employed a JEOL 2100F microscope and an accelerating voltage of 200 kV (with a point resolution of 0.19 nm).

3. Results and discussion

3.1. XRD

Fig. 1 presents the diffraction patterns of samples a–f, obtained under different synthesis conditions. Fig. 1a and Table 1 show the samples that were synthesized at a temperature of 40 °C, indicating that both samples exhibited peaks with Miller indexes of 100, 200 and 210, corresponding to 2.87–2.88°, 4.86–4.88°, and 5.54–5.56° (2θ), respectively, for hexagonal SBA-3 [25]. Fig. 1b shows diffraction patterns for different samples synthesized at 70 °C and 10 °C with different aging times and CTAB/TEOS and HCl/TEOS ratios. It can be seen that SBA-3 structure characteristics were not obtained under these conditions, based on the poor definitions and shifts of the signals corresponding to [100] and the absence of signals indicating long-range regularity. We have calculated a_0, the unit cell parameter, from the intensity of the [100] signal of each diffraction pattern, which corresponds to the hexagonal mesophase characteristic of the SBA-3 material, using the following equation: $a_0 = 2d_{100}/\sqrt{3}$ (Table 1), and the results show little variation between SBA-3a and SBA-3b, indicating that the samples obtained are of good purity.

3.2. BET

Fig. 2 shows the N_2 sorption–desorption isotherms and the corresponding pore size distribution curves of the SBA-3a and SBA-3b samples. Both samples exhibit typical type-IV isotherms. When the relative pressure P/P_0 is between 0.2 and 0.3, the isotherm exhibits a sharp step, indicating capillary condensation within the mesopores. The very slow linear increase obtained when a higher pressure is employed (>0.3 P/P_0) indicates adsorption on the outer

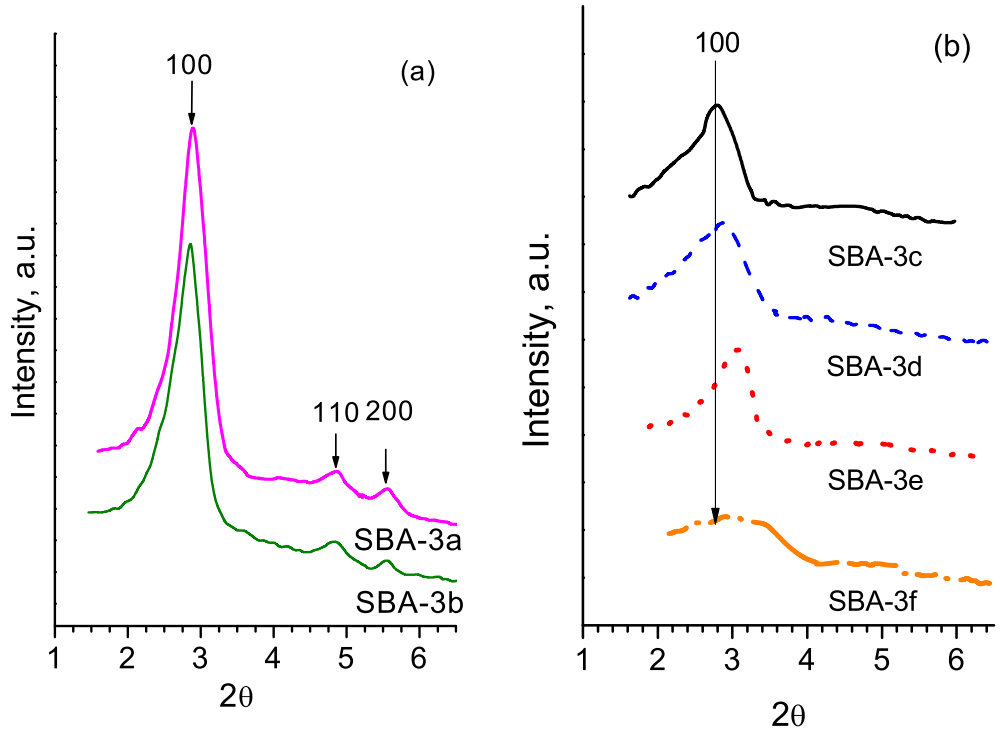

Fig. 1. XRD patterns of samples synthesized at: a) 40 °C and b) 70 °C and 10 °C, at different, CTAB/TEOS, HCl/TEOS molar ratios and aging time: SBA-3a (0.069-9.07-40-0); SBA-3b (0.17-4.54-40-24); SBA-3c (0.17-9.07-70-0); SBA-3d (0.17-9.07-70-24); SBA-3e (0.069-9.07-10-12); SBA-3f (0.27-9.07-10-12.

SBA-3 surface, which demonstrates no hysteresis loop between adsorption and desorption branches. At the same relative pressure, the SBA-3a sample demonstrates more absorption than the SBA-3b sample. Surface areas, pore volumes and pore sizes are shown in Table 1.

3.3. TEM

In addition to the SBA-3a XRD results, the TEM images displayed in Fig. 3A and B clearly show well-ordered hexagonal arrays along the [110] and [100] directions.

3.4. Experimental design-response surface

To analyze simultaneous variations in the factors considered, the experimental design facilitates the synthesis of materials with optimal textural properties and optimizes the conditions employed for synthesis. RSM is used in the present work to model and optimize the response intensity of the XRD pattern for the [100] signal during SBA-3 synthesis. Table 2 shows the complete Box–Behnken designs utilized for all samples.

For each effect, variance analysis (ANOVA) [26] partitions the variability of response into separated pieces. Subsequently, ANOVA is used to determine the statistical significance of each effect by

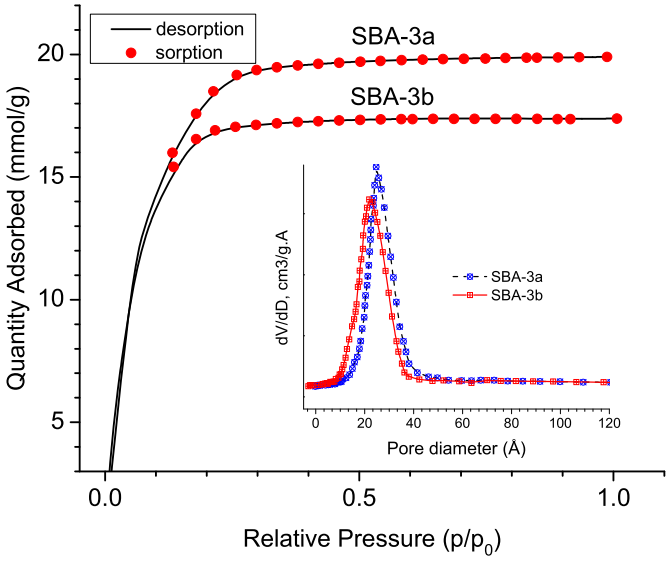

Fig. 2. N_2 sorption isotherms of the two samples synthesized at 40 °C and at different aging times, CTAB/TEOS and HCl/TEOS molar ratios (Table 1).

Table 1
Physicochemical properties of SBA-3 synthetized at 40 °C.

Sample	d100 (Å)	a_0 (Å)	SBET (m^2/g)	Pore volume (cm^3/g)[a]	Pore diameter (nm)[a]
SBA-3a	31.30	36.62	1110.7	0.36	2.50
SBA-3b	31.26	36.14	1013.5	0.32	2.20

SBA-3a: (0.069-9.07-40-0); SBA-3b: (0.17-4.54-40-24).
[a] BJH adsorption average pore diameter and pore volume.

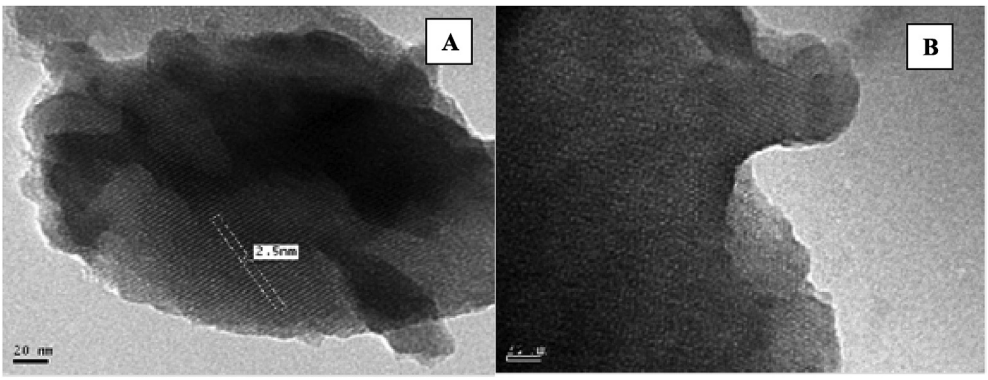

Fig. 3. TEM micrographs along [110] and [100] directions of SBA-3a sample, synthesized at 40 °C and using TEOS: 0.069 CTAB: 9.07 HCl: 138.9H_2O reaction mixture molar composition.

comparing the mean square against an estimate of the corresponding experimental error.

In this case, the ANOVA results (Table 3) show that the following variables exert significant influences on the intensities obtained: quadratic effects of CTAB/TEOS, HCl/TEOS and temperature (95.0% confidence levels), and the lineal effect of temperature (90.0% confidence level).

The p-value is defined as the probability of obtaining a result equal to or "more extreme" than what was actually observed, assuming that the null hypothesis is true. If the p-value is less than or equal to the chosen significance level (α), the test suggests that the observed data are inconsistent with the null hypothesis, such that the null hypothesis must be rejected [18,19].

The R-squared statistic [19] indicates that the model accounts for 90.51% of the variability in intensity. Here, this value indicates that the model explains 90.51% of the total variations.

Table 2
The complete Box–Behnken design.

Factors				Response
A CTAB/TEOS	B HCl/TEOS	C temperature	D time	Intensity[a]
0.171	9	10	12	4600
0.171	9	10	24	4800
0.068	4.4	40	12	5500
0.068	13.6	40	12	6400
0.171	9	40	12	10,000
0.274	4.5	40	12	5000
0.274	13.6	40	12	5800
0.171	9	70	0	3000
0.171	9	70	24	3300
0.171	4.5	10	12	3500
0.171	13.6	10	12	4700
0.068	9	40	12	12,000
0.171	9	40	12	10,000
0.274	9	40	12	6500
0.068	9	40	24	10,000
0.274	9	40	24	7500
0.171	4.5	70	12	1000
0.171	13.6	70	12	2500
0.068	9	10	12	4500
0.274	9	10	12	4000
0.171	13.6	40	0	7000
0.171	4.5	40	12	5700
0.171	9	40	12	10,000
0.171	4.5	40	24	11,000
0.171	13.6	40	24	9000
0.068	9	70	12	2000
0.274	9	70	12	1500

[a] Normalized Units for XRD signal corresponding to [100] Miller index.

Table 3
ANOVA test.

Source	Sum of squares	Df	Mean square	F-ratio	P-value
A: CTAB/TEOS	$5.776E^6$	1	$5.776E^6$	2.47	0.1471
B: HCl/TEOS	$2.595E^6$	1	$2.595E^6$	1.11	0.3177
C: Temperature	$8.436E^6$	1	$8.436E^6$	3.61	0.0867
D: time	$3.881E^6$	1	$3.881E^6$	1.66	0.2266
AA	$1.378E^7$	1	$1.378E^7$	5.89	0.0356
AB	2500.0	1	2500.0	0.00	0.9746
AC	0.0	1	0.0	0.00	1.0000
AD	400167.0	1	400167.0	0.17	0.6878
BB	$2.3094E^7$	1	$2.3094E^7$	9.88	0.0105
BC	22500.0	1	22500.0	0.01	0.9238
BD	$1.982E^6$	1	$1.982E^6$	0.85	0.3789
CC	$1.651E^8$	1	$1.651E^8$	70.60	0.0000
CD	248743.0	1	248743.0	0.11	0.7510
DD	276049.0	1	276049.0	0.12	0.7383
Total error	$2.338E^7$	10	$2.33821E^6$		
Total (corr.)	$2.464E^8$	26			

R-squared = 90.5092% R-squared (adjusted for d.f.) = 79.4367%.

Pareto chart shows, the parameters that produce a more pronounced effect on the Intensities (Fig. 4).

The model equation by which the response surfaces were fitted to experimental data points is represented as follows:

Intensity = 9866,42−919,239 * Temperature − 1624,81 * $(CTAB/TEOS)^2$ − 2021,14 * $(HCl/TEOS)^2$ − 5403,78 * $(Temperature)^2$

Fig. 5 shows the contours of the estimated response surface products of the design.

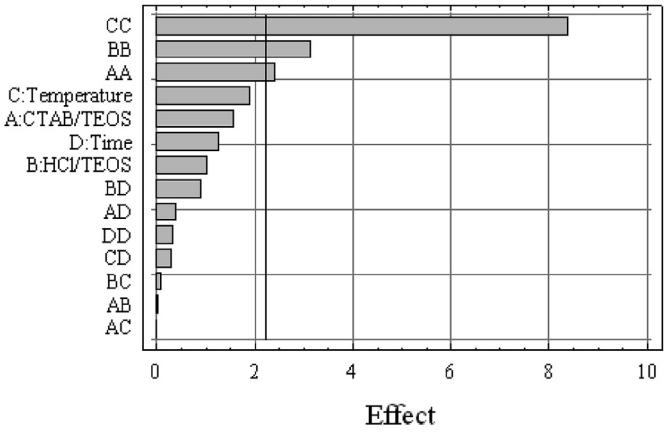

Fig. 4. Pareto chart.

Fig. 5 shows the interaction between factors required to obtain maximum intensity for the characteristic XRD signal for the SBA-3 material utilized in the present study. According to the figures contained herein, optimal experimental conditions are represented by the dark red zone, in which the CTAB/TEOS ratio is between 0.10 and 0.17 and the temperature is between 35 and 42 °C (Fig. 5A); the HCl/TEOS ratio is between 7 and 11 and the temperature is between 30 and 45 °C (Fig. 5B); the CTAB/TEOS ratio is between 0.068 and 0.11 and the HCl/TEOS ratio is between 8 and 10 (Fig. 5C); and the temperature is between 35 and 45 °C and the aging time is between 12 and 24 h (Fig. 5D).

Based on the experiments detailed herein, the most important factor for achieving hexagonal 2D mesoporous structure is temperature. The best results were obtained at 40°°C without exception, although some good results were obtained at 10 °C. No ordered hexagonal mesoporous structures were achieved at 70 °C. This behavior can be understood by considering the influence of temperature on quaternary ammonium surfactant packaging; this variable directly affects the volume of the hydrophobic tail of the surfactant and, therefore, the effective surfactant shape. Medium synthesis temperatures favor a hexagonal periodicity of P6mm.

As the temperature is increased, the disorder in the surfactant tail increases, increasing the surfactant molecular packing volume and disorganizing the rod-like packing.

Regarding the influence of surfactant concentration, high CTAB concentrations did not favor hexagonal pore arrangement.

While surfactant packing appears to be the driving force for rearrangement, significant kinetic barriers remain in the synthesis of mesoporous materials, for instance, the hydrolysis and condensation reactions of the siliceous precursor employed. Hydrolysis occurs by nucleophilic attack of oxygen in the water molecule over the silicon atom, as evidenced by the reaction of isotopically labeled water with TEOS, which produces only unlabeled alcohol both in acid and basic media [27]. Hydrolysis is more rapid and complete when catalysts such as mineral acids are employed [28]. Our experimental results show that higher amounts of acid induce the formation of SBA-3 structures (HCl/TEOS molar ratio = 8–11). This is because the siliceous precursor is not completely hydrolyzed in

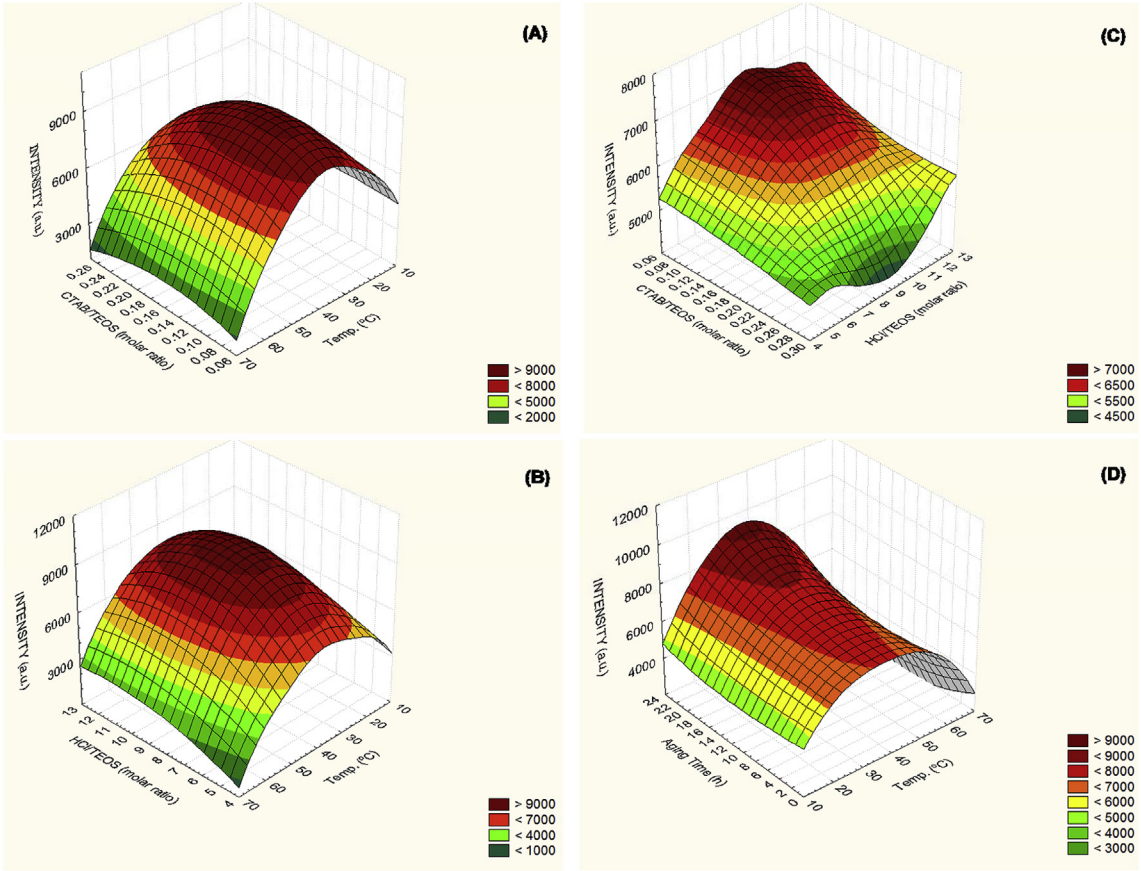

Fig. 5. Contour of response surface fitted for the design. Intensity as a function of the (a) CTAB/TEOS molar ratio and temperature, (b) HCl/TEOS molar ratio and temperature, (c) CTAB/TEOS molar ratio and HCl/TEOS molar ratio and (d) aging time and temperature.

Table 4
Synthesis of SBA-3 in the optimal conditions.

	CTAB/TEOS	HCl/TEOS	Temp.(°C)	Aging time (h)	SBET (m^2/g)	Pore diameter (nm)	Intensity[a]
SBA-3op1	0.07	9	35	24	1220	1.99	11,800
SBA-3op2	0.10	10	40	12	1330	2.10	13,500
SBA-3op3	0.16	9	45	12	1175	2.03	12,300

[a] Normalized Units for XRD signal corresponding to [100] Miller index.

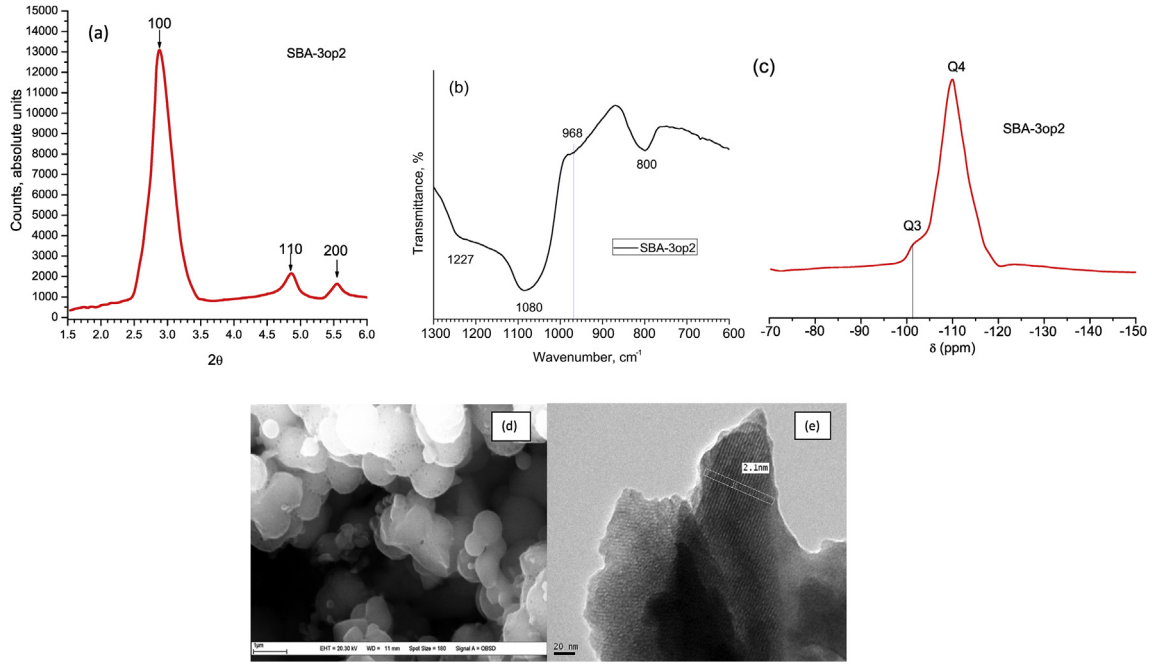

Fig. 6. (a) XRD (b) FTIR in the finger print zone, (c) ^{29}Si NMR-MAS, (d) SEM and (e) TEM for SBA-3op2 optimized sample.

lower HCL concentrations, resulting in lower rates of hydrolysis and condensation.

The statistical methodology followed in this work enabled us to define operation conditions for this reaction that optimize SBA-3 synthesis. The best operation conditions obtained were as follows:

(A) CTAB/TEOS molar ratio: 0.07 and 0.16
(B) HCl/TEOS molar ratio: 8 and 11
(C) Temperature of synthesis: 35 and 45 (°C)
(D) Aging time of synthesis: 12–24 (h)

To corroborate these results and conclusions, several reactions were performed using these optimal conditions. Table 4 shows the optimal synthesis conditions as determined by statistical analyses.

The optimum sample obtained by applying the experimental design thus determined was characterized using XRD, FTIR, 29Si NMR-MAS, SEM and TEM (see Fig. 6a–e). Fig. 6a displays the XRD pattern of optimized sample SBA-3op2 and displays three characteristic well-defined signals for the high-purity SBA-3 sample. The FTIR spectrum of the optimized sample (Fig. 6b) shows the characteristic bands of a siliceous SBA-3-type material [29,30], exhibiting a major band at 1080 and a shoulder at 1227 cm^{-1}, corresponding to Si–O–Si asymmetric internal and external stretching modes, respectively. The weaker band observed at 800 cm^{-1} is due to symmetric Si–O–Si stretching. It is worth noting that the very low intensity of the signal assigned to the Si(OH) stretching mode at 968 cm^{-1} s indicates high purity and structural regularity. Fig. 6c shows the ^{29}Si MAS NMR spectra of the SBA-3op2 sample, in which a very high signal at −111 and a low signal at −101 ppm can be seen. These two peaks corresponding to $[Si(OSi)_4]$ and $[Si(OSi)_3OH]$, (Q^4 and Q^3), respectively [31,32], and therefore, support the data obtained by FTIR.

The SBA-3 particle size was 0.8–1.3 μm in diameter, almost spherical, indicating a highly ordered structure with few imperfections and without other phases in the outer surface (Fig. 6d). TEM results indicate that the ordered porous nanostructure has an average 2.1-nm pore diameter, as shown in Fig. 6e for the SBA-3op2 sample.

Thus, the samples obtained possess high purity and excellent structural regularity, based on the characterization methodology applied.

4. Conclusions

This study utilized experimental design to optimize the synthesis conditions used to prepare SBA-3 nanostructured materials. Utilizing these optimal conditions, we observed the intensity of the XRD signal at [100] and the other two peaks at long angles indexed at [110] and [200] for the most crystalline SBA-3 material synthesized. According to the statistical methodology applied in this work, the CTAB/TEOS and HCl/TEOS ratios and synthesis temperature exert the most profound influences on the synthesis of highly ordered SBA-3 material.

Acknowledgments

JC, MLM, ARB and OAA are researchers from CONICET; MVP and LPR are research fellows from CONICET. The authors thank CONICET Argentina, PIP CONICET 11220120100218CO. 2014–2016.

References

[1] T. Yanagisawa, T. Shimizu, K. Kuroda, K. Kato, Bull Chem Soc Jpn 63 (1990) 988–992.
[2] C. Kresge, M. Leonowicz, W. Roth, J. Vartuli, J. Beck, Nature 359 (1992) 710–712.
[3] Chiola V, Ritsko J, Vanderpool C. US Patent 3 (1971) 556–725.
[4] J. Beck, J. Vartuli, W. Roth, M. Leonowicz, C. Kresge, K. Schmitt, C. Chu, D. Olson, E. Sheppard, S. McCullen, J. Higgins, J. Schlenker, J Am Chem Soc 114 (1992) 10834–10843.
[5] J. Beck, J. Vartuli, G. Kennedy, C. Kresge, W. Roth, S. Schramn, Chem Mater 6 (1994) 1816–1821.
[6] S. Rani, K. Sumanjit, R. Mahajan, Desalin Water Treat (2014).
[7] J. Goscianska, A. Olejnik, R. Pietrzak, Mater Chem Phys 142 (2013) 586–593.
[8] K. Han, L. Ma, H. Zhao, X. Li, Y. Chun, J. Zhu, Microporous Mesoporous Mater 151 (2012) 157–162.
[9] M. Khayoon, B. Hameed, Appl Catal A General 460–461 (2013) 61–69.
[10] A. Inayat, A. Kuhnt, W. Schwieger, W. Einicke, J. Kullmann, D. Enke, J Porous Mater 18 (2011) 767–777.

[11] M. Anbia, S. Salehi, Dyes Pigments 94 (2012) 1–9.
[12] A. Held, J. Kowalska-Kuś, K. Nowińska, Catal Commun 17 (2012) 108–113.
[13] J. Patarin, B. Lebeau, R. Zana, Curr Opin Coll Int 7 (2002) 107–115.
[14] D. Zhao, Q. Huo, J. Feng, F. Chmelka, G. Stucky, J Am Chem Soc 120 (1998) 6024–6032.
[15] P. Albouy, A. Ayral, Chem Mater 14 (2002) 3391–3397.
[16] J. Lee, S. Joo, R. Ryoo, J Am Chem Soc 124 (2002) 1156–1157.
[17] G. Box, K. Wilson, J R Stat Soc Ser B 13 (1951) 1–45.
[18] R. Fisher, The design of experiments, second ed., vol. 32, 1937, pp. 218–219.
[19] D. Montgomery, Design and analysis of experiments, third ed., John Wiley &Sons, Inc, New York, 1991.
[20] S. Ferreira-Dias, A. Correia, F. Baptista, M.M.R. da Fonseca, J Mol Catal B Enzym 11 (2001) 699–711.
[21] O.A. Anunziata, A.R. Beltramone, J. Cussa, Appl Catal A General 270 (2004) 77–85.
[22] G. Du, Y. Yang, W. Qiu, S. Lim, L. Pfefferle, G. Haller, Appl Catal A General 313 (2006) 1–13.
[23] M. Sen, H. Shan, Robot Comput Integr Manuf 23 (2007) 17–24.
[24] O.A. Anunziata, A.R. Beltramone, M.L. Martinez, L. López Belon, J Coll Interface Sci. 315 (2007) 184–190.
[25] M.L. Martínez, M.V. Ponte, A.R. Beltramone, O.A. Anunziata, Mater Lett 134 (2014) 95–98.
[26] R. Kuehl, Design of experiments, second ed., Duxbury-Thomson Learning, Pacific Grove, 2000.
[27] C.J. Brinker, Hydrolysis and condensation of silicates: effects on structure, J Non Cryst Solids 100 (1988) 31–50.
[28] M. Vorankov, V. Mileshkevich, Y. Yuzhelevski, The Siloxane Bond, London Consultants Bureau, New York, 1978.
[29] O.A. Anunziata, M.L. Martínez, M. Gomez Costa, Mater Lett 64 (2010) 545–548.
[30] D.A. Neumayer, E. Cartier, J Appl Phys 90 (2001) 1801–1808.
[31] E. Janiszewska, Microporous Mesoporous Mater 193 (2014) 77–84.
[32] A. Grünberg, H. Breitzke, G. Buntkowsky, Spectrosc Prop Inorg Organomet Compd 43 (2012) 289–323.